A Polarimetric Survey of Radio-Frequency Interference in C- and X-Bands in the Continental United States Using WindSat Radiometry

Steven W. Ellingson, *Senior Member, IEEE,* and Joel T. Johnson, *Senior Member, IEEE*

***Abstract*—Transmissions from ground-based systems in C- and X-bands present a significant challenge to the use of these bands for passive microwave remote sensing from aircraft and satellites. Because future missions plan to continue to use these frequencies, it is important to characterize and understand the nature of interference in as much of the candidate spectrum as possible. This paper presents a statistical analysis of interference observed in the continental U.S. using six months of data collected from the C- and X-band channels of the WindSat microwave radiometer. Our findings are consistent with those of previous studies by Li *et al.* and Njoku *et al.*, which are based on data obtained from the Advanced Microwave Scanning Radiometer-EOS using somewhat similar center frequencies and bandwidths. Results show significant radio-frequency interference (RFI) at C-band, including brightnesses in horizontal and vertical polarizations in excess of 330 K, while X-band RFI is less obvious through direct examination of measured linearly polarized brightnesses. Evidence of lower levels of RFI is provided through use of the spectral and polarization indexes of Li *et al.*, which reveal likely RFI contributions at X-band as well. Further confirmation of X-band RFI is obtained through analysis of the polarimetric channels, which are shown to provide direct evidence of RFI in contrast to the linearly polarized channels. A temporal analysis of the largest C-band RFI sources is also provided in an attempt to further understand their properties.**

***Index Terms*—Land remote sensing, microwave radiometry, radio-frequency interference (RFI).**

I. Introduction

ACCESS to spectrum in C- and X-bands is essential for passive microwave remote sensing of the Earth from air- or spaceborne platforms. Legitimate transmissions from ground-based systems are already known to present a significant challenge to the use of these bands for remote sensing. The problem for spaceborne systems has been initially characterized in the 6.925- and 10.65-GHz channels of the Advanced Microwave Scanning Radiometer-EOS (AMSR-E), which have bandwidths of 350 and 100 MHz, respectively [1], [2]. With an integration time of 2.6 ms and instantaneous fields of view (IFOV) of 43×75 km and 27×48 km for C- and X-bands respectively, both frequencies were found to be significantly limited by radio-frequency interference (RFI). Some RFI was strong enough to be detected as excessively high brightness temperatures. However, additional RFI too weak to be detected as excess brightness temperature was revealed by other methods. For example, it was shown that weak RFI could be identified by geophysically unexpected "spectral index values" — i.e., differences in observed brightness between C- and X-band channels—or by unexpectedly large "polarization indexes"—i.e., evidence of strong polarization. In addition, consideration of both annual means and standard deviations of the spectral index was proposed in [2] as a possible method for producing an RFI "mask" for excluding contaminated regions from geophysical retrieval analyses.

Because future missions will use similar frequencies and bandwidths [3], it is desireable to characterize and understand the nature of RFI in as much of the candidate spectrum as possible. One outcome of such studies is related to the development of improved methods for eliminating RFI corrupted data, particularly data containing low-level RFI contributions, from geophysical analysis of measured brightnesses in post-processing. Although the studies of this paper are indirectly related to this goal, the focus of the current paper is on understanding properties of RFI sources themselves, including their temporal, spectral, and polarization properties, as well as their spatial distribution. Such knowledge of the RFI environment as observed from space is critical for the development of new technologies for real-time interference mitigation in future spaceborne radiometers.

To contribute to this understanding, an analysis of RFI observed in six months of observations in the C- and X-band channels of WindSat is provided in this paper. WindSat is an Earth-orbiting polarimetric radiometer with characteristics which are similar but not identical to AMSR-E [4]. It is the primary payload on the U.S. Department of Defense Coriolis satellite, which was launched in January 2003 and is now in an 840-km circular sun-synchronous orbit. The WindSat C-band channel is centered at 6.8 GHz with a 125-MHz bandwidth, a 5-ms integration time, and a 40×60 km IFOV in vertical (V) and horizontal (H) polarizations. The X-band channel is centered at 10.7 GHz with a 300-MHz bandwidth, 3.5-ms integration time, and a 25×38 km IFOV, measuring V, H, and the third and fourth Stokes parameters, referred to as "U" and "4" in this paper. Thus, WindSat observes somewhat different segments of the C- and X-band spectrum, and, in contrast to AMSR-E, is fully polarimetric at X-band. The WindSat frequency channel at C-band is approximately the same as the lower third of the

Manuscript received January 13, 2005; revised June 28, 2005. This work was supported by the National Polar-orbiting Operational Environmental Satellite System Integrated Program Office.

S. W. Ellingson is with the Bradley Department of Electrical and Computer Engineering, Virginia Polytechnic Institute and State University, Blacksburg, VA 24061 USA (e-mail: ellingson@vt.edu).

J. T. Johnson is with the Department of Electrical and Computer Engineering and ElectroScience Laboratory, The Ohio State University, Columbus, OH 43210 USA.

Digital Object Identifier 10.1109/TGRS.2005.856131

AMSR-E C-band channel; if RFI sources are nonuniformly distributed in frequency, this small bandwidth could be expected to modify the total amount of RFI observed compared to AMSR-E, and also can be viewed as providing improved spectral resolution when attempting to classify particular RFI source frequencies. The WindSat X-band channel is about three times wider than the corresponding AMSR-E channel, again indicating that RFI differences are likely at X-band for WindSat compared to AMSR-E. The availability of fully polarimetric X-band data from WindSat provides additional opportunities for detection and characterization of RFI.

WindSat observations of the continental U.S. and coastal waters from the months of September 2003 through February 2004 are utilized. This spatial region is attractive for analysis due to the public availability of information on many ground-based transmitters in C- and X-bands, so that "matchups" of source information with WindSat data can be performed in the future. Also, a study of C- and X-band RFI based on these databases has already been performed, and the results of this paper can be compared against existing simulations [5].

Following an approach similar to that in [1] and [2], we search for RFI using excess absolute brightness temperature as well as unexpected spectral and polarization index values. In order to present a concise characterization of this large dataset, we use maps of mean and extreme (maximum/minimum) values. The extreme value cases are useful in producing conservative spatial maps of possible RFI locations for use in future matchup studies. Comparison of mean and extreme metrics also provides some insight into temporal behavior (i.e., intermittency). We extend this approach by exploiting fully polarimetric measurements at X-band to reveal additional RFI and evidence of preferred directions of emission in RFI detections. A related effort analyzing RFI in WindSat data on a global scale is also in progress [6]; however, the goals of the two studies are distinct in that the related effort is focused on RFI removal for retrieval applications rather than on analyses of RFI statistical properties as in this paper.

II. Methodology

WindSat "sensor data records" (SDRs) for the period September 2003 to February 2004 are used in this study; the SDR data are from data release 1.6.1 These data have been calibrated following the process described in [4], and include an antenna pattern correction operation in order to produce accurate third and fourth Stokes brightnesses. Because the WindSat antenna feeds have slightly different instantaneous fields of view, a collocation and resampling process is utilized in generating the SDR brightnesses. This implies that the brightness results presented are not instantaneous observations, but rather have been interpolated among nearby observations in the resampling process. In addition, the data considered here are averaged to the resolution of the C-band channel; this is implies that the X-band data illustrated are additionally spatially averaged beyond the original X-band antenna beam pattern.

For this analysis, the data are spatially requantized to a grid which is rectilinear in latitude and longitude. Each point in the grid defines a pixel for which the brightness temperature statistics are computed. The grid has spacing equal to four times the mean spacing of the swath data obtained from the 1.6.1 SDRs. A significant spatial overlap in both the original and requantized data remains due to oversampling in the SDR data, particularly in the along-track direction (mostly in latitude for the WindSat orbit.) The chosen factor of four is desirable in that small spacings tend to produce results that are somewhat redundant (being finer than the resolution of the instrument), whereas larger spacings reduce the spatial resolution of the data beyond that achieved by the instrument. The resulting grid has a spacing of 0.124° in latitude and 0.568° in longitude, and contains 210 $\times$ 105 points in the region 24° to 48° north latitude, 65° to 125° west longitude.

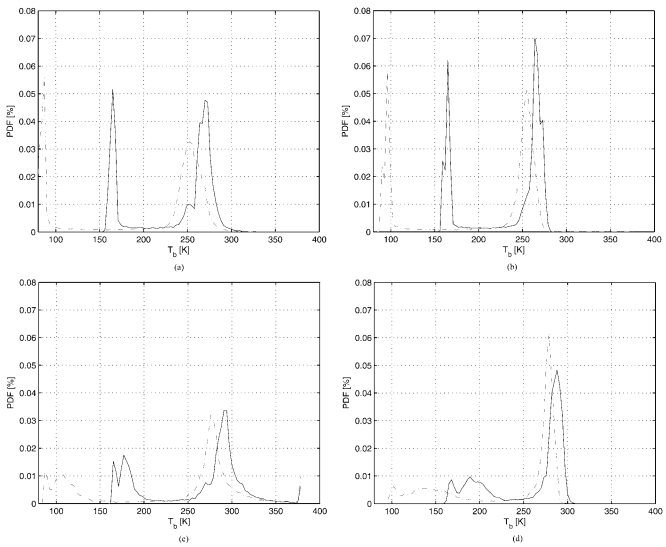

Fig. 1. Probability density functions of C- and X-band brightnesses. (Solid line) V. (Broken line) H. (a) C-band, mean. (b) X-band, mean. (c) C-band, max. (d) X-band, max.

Due to WindSat orbit, antenna, and swath properties, the "duty cycle" of observation for any given point on the Earth is very low. To verify that the sampling was at least approximately uniform over the surface of the Earth, we calculated the probability density function (pdf) of the number of observations per grid point. An "observation" was defined as follows: for each SDR, the grid point nearest the record geophysical location was determined, and then this grid point (and no other) was declared to have been observed. We found that each grid point was observed at least 500 times over the six-month period; i.e., ~ 3 times/day on average, and that all grid points were sampled between 500 and 600 times over that period. Thus, the results for all grid points observed should have roughly the same statistical significance.

III. Spatial Statistics

A. Linearly Polarized Channels

Linearly polarized brightness temperatures observed on the surface of the Earth in both C- and X-band can be expected to remain within the range 70–330 K, with 330 K being an extremely high upper limit for geophysical possibility. For the purposes of this paper, temperatures greater than 330 K are considered unambiguous RFI; this limit also corresponds to the highest brightness temperature the WindSat radiometer can accurately measure.

An initial examination of the gridded dataset is provided in Fig. 1, where pdfs of the mean and maximum linearly polarized brightnesses computed over the grid defined in the previous section are illustrated. Land and sea contributions in these plots are obvious, and there is no particular evidence of RFI visible except for the dramatic spike at the high end of the C-band "max" pdf. These plots show that the possible range of variations in geophysical brightnesses is large, making low-level RFI difficult to detect.

Fig. 2 shows the mean and maximum C-band brightness temperatures, displayed as a flat-shaded contour plot, for the entire six-month dataset and for both polarizations. The maximum operation essentially attempts to locate all evidence of large C-band RFI throughout the six-month period; information on the temporal variability of the sources located is not available in this plot. However, by comparing the mean and max plots, information on the average temporal behavior can be obtained: sources of persistent RFI will appear strong both in the mean and max plots, while more temporally intermittent sources will appear much weaker in the mean. All plots show clear evidence of nongeophysical brightness temperature distributions in the form of localized "hot spots," which are not expected to occur naturally. Furthermore, many of these hot spots exhibit unnaturally bright maximum temperatures (in excess of 330 K) making it almost certain that they are due to anthropogenic RFI. As in [1] and [2], there also seems to be some correlation between hot spots and population centers, although this association is weak, and many large cities show no evidence of a corresponding hot spot. Comparison of the max and mean values shows that both persistent and more intermittent sources are observed. Results in the two polarizations are similar, although apparent RFI regions with large polarization differences in the max values are observed.

Mean observations over sea regions in Fig. 2 show no RFI evidence, but features in the max results do indicate some variability in sea observations. However, a closer observation of the features in the H pol max plot [Fig. 2(b)] show that the larger brightnesses observed are associated with hurricane Isabel, which moved from the Atlantic toward the coast of North Carolina during the period September 6–13, 2003. Once these data are removed, no obvious evidence of at-sea RFI is obtained.

Similar plots for X-band V and H polarizations are illustrated in Fig. 3. The results are dramatically different from C-band, in that no obvious RFI is immediately apparent, either in mean or max plots. Note the AMSR-E studies [1] and [2] also indicate minimal X-band RFI in the U.S., although strong X-band RFI was observed in other global regions. These results are somewhat surprising given the larger bandwidth of the WindSat X-band channel compared to AMSR-E. However the absence of obvious RFI in Fig. 3 does not necessarily indicate that no RFI is present. Note the features associated with hurricane Isabel observed at C-band remain apparent the max plots as well.

Next, we consider extreme values of the spectral index, defined in this analysis as the observed brightness temperature at C-band minus the observed brightness temperature at X-band. This index is normally < 5 K for the geophysical signal, and is typically negative. A spectral index ≥ 5 K provides evidence of C-band RFI. The maximum and minimum of the spectral index are shown in Fig. 4 for vertical and horizontal polarizations. Note the max plot here captures C-band excess emission, because the spectral index is a signed quantity, while the min plot captures X-band excess emission; atmospheric effects produce the strong min values observed in X-band horizontal results over the sea. Comparisons with the absolute brightness temperature results shown previously suggest that the spectral index may be a more sensitive test for RFI, as originally found in [1] and [2], due to the elimination of some geophysical variability when the difference is computed. Evidence of X-band sources is easily observed in these plots, although again the number of sources appears smaller than at C-band. Methods for developing an RFI mask based on the mean and standard deviation of the spectral index have been presented in [2]; no method for removing RFI from particular observations, rather than through a masking procedure for a large set of observations, has been verified.

Finally, we consider extreme values of the polarization index P, defined as

$$P = \frac{T_{B,H} - T_{B,V}}{T_{B,H} + T_{B,V}} \tag{1}$$

where $T_{B,H}$ and $T_{B,V}$ are the brightness temperatures of the H and V polarizations, respectively. The extreme values of $P = +1$ and $P = -1$ correspond to observations which are completely H-polarized or completely V-polarized, respectively. Since geophysical signals over land are normally only weakly polarized, a large positive or negative value of P suggests anthropogenic RFI. Fig. 5 plots the observed maximum and minimum values P over the entire six-month dataset; note the values illustrated are the base-ten logarithm of the result. The C-band channel results show evidence of both unnatural horizontal and vertical polarization, some of it coincident with RFI hot spots observed above. Sources with excess horizontal polarization are more numerous, while vertical excess values are more difficult to classify due to the strong vertical polarization associated with bodies of water. X-band shows similar results although to a much smaller scale than at C-band. Note the color scales at X-band have been modified in order to enhance contrast in the plots.

B. X-Band Correlation Channels

Fig. 6 illustrates the mean and max X-band brightness temperatures for the correlation channels "U" and "4." For geophysical sources, these channels respond to the degree of azimuthal asymmetry of the medium under view, and the magnitude and sign of the brightness measured depends on the relative azimuth orientation between the medium and the satellite azimuthal observation angle. The values of the correlation channels due to geophysical mechanisms may be either positive or negative, but in either case are expected to be very small for land regions. For this reason, statistics of the magnitudes of these channels were computed, so that RFI could be more easily identified as a large value. A notable feature in Fig. 6 is the apparent high brightness coincident with coastlines in the $|4|$ results. This is thought to be due to a slight misalignment of the left and right

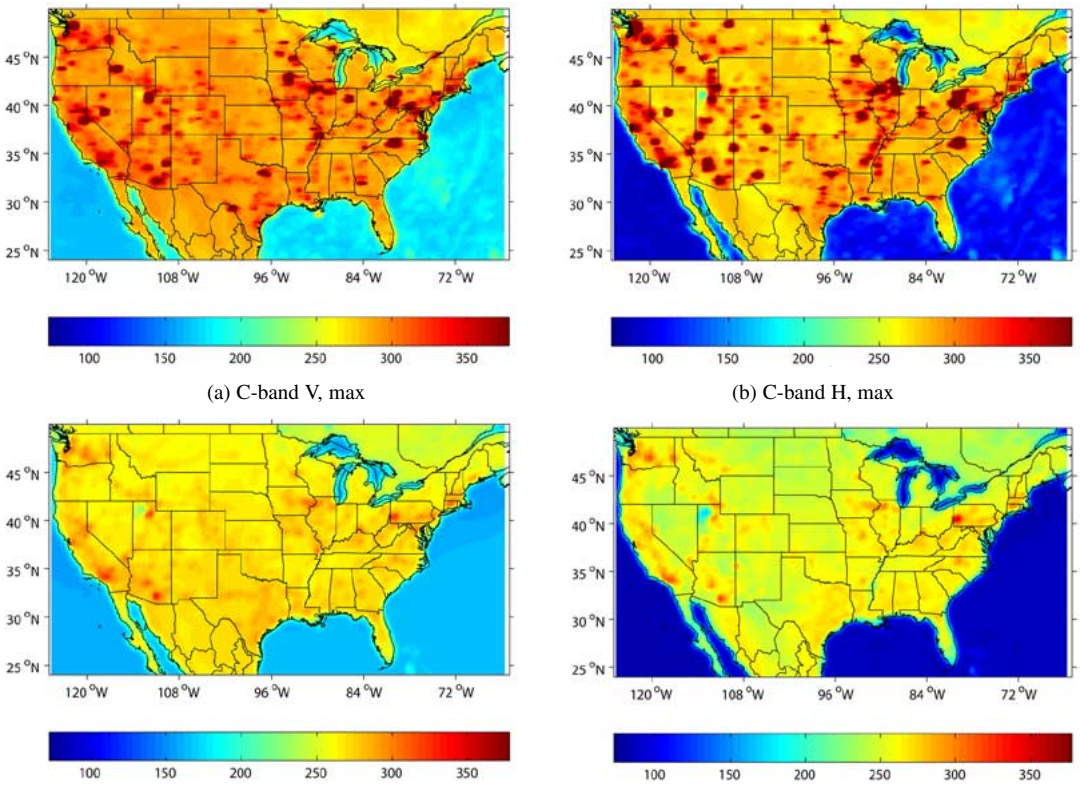

(a) C-band V, max (b) C-band H, max

(c) C-band V, mean (d) C-band H, mean

Fig. 2. C-band brightness temperature maximum and mean values, in Kelvin.

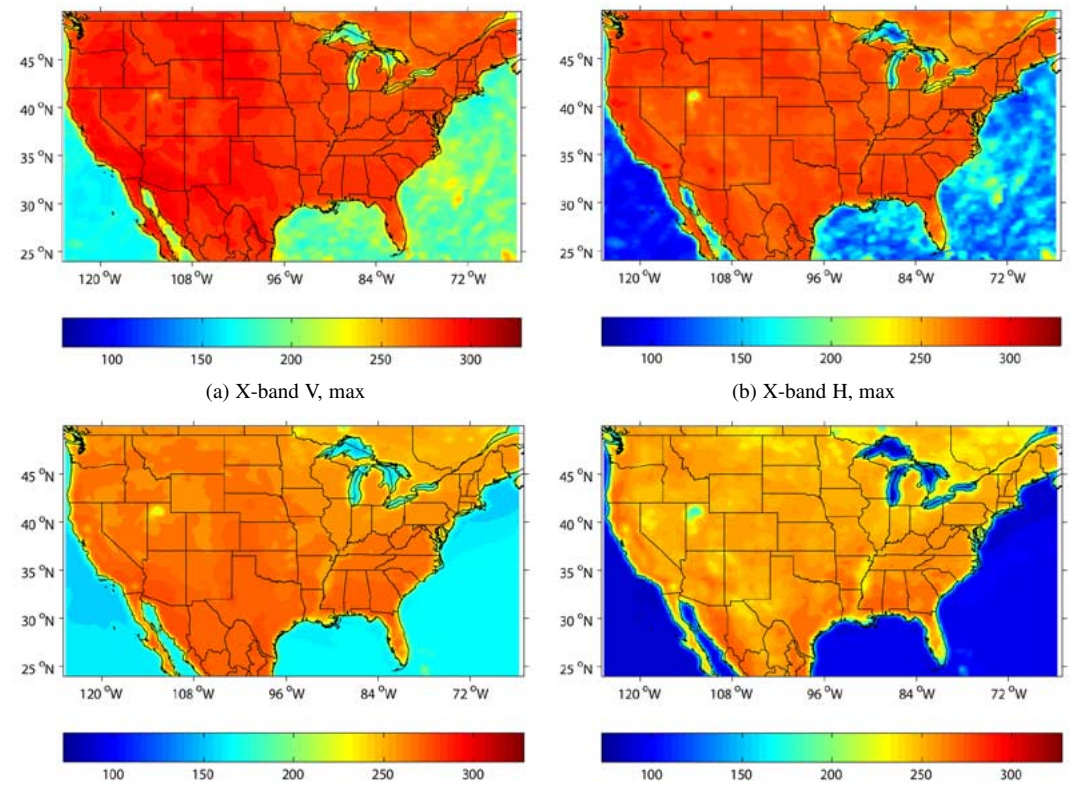

(a) X-band V, max (b) X-band H, max

(c) X-band V, mean (d) X-band H, mean

Fig. 3. X-band brightness temperatures (linear polarizations) max and mean values, in Kelvin.

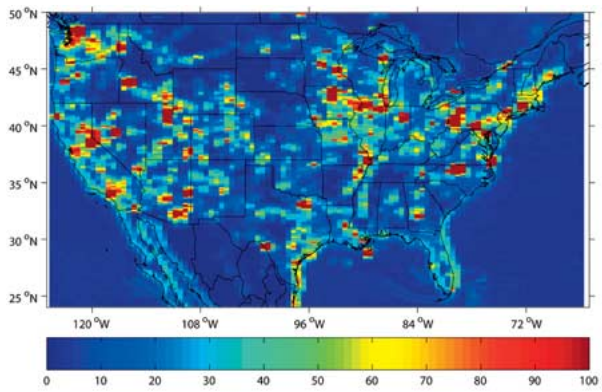

(a) Vertical polarization, max

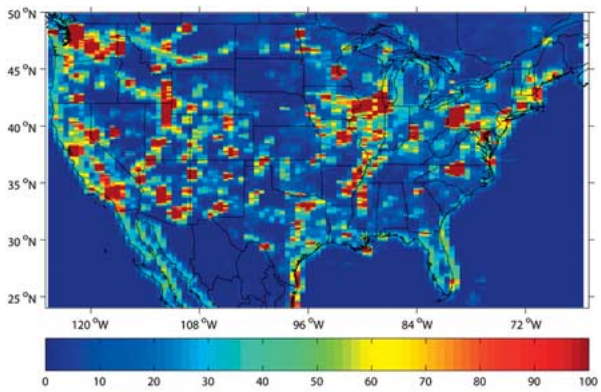

(b) Horizontal polarization, max

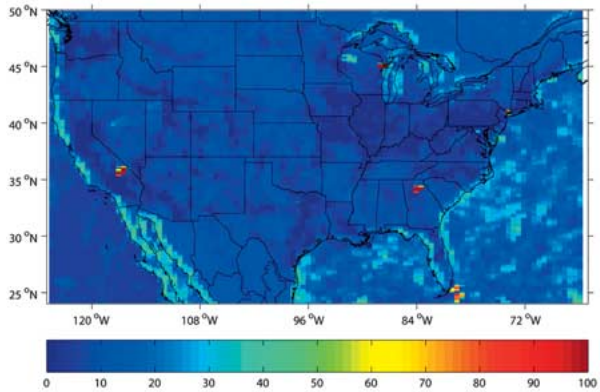

(c) Vertical polarization, amplitude of min

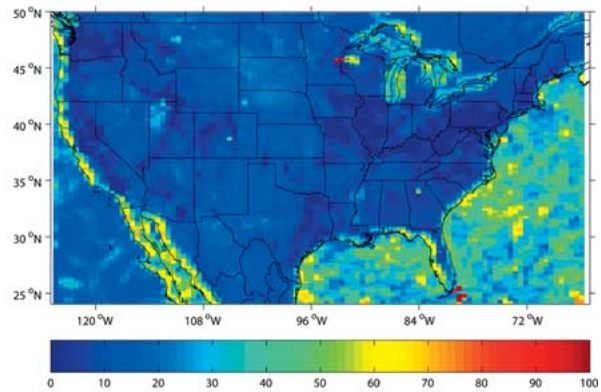

(d) Horizontal polarization, amplitude of min

Fig. 4. Max and min maps of the spectral index (C-band brightness temperature minus the X-band brightness temperature), in Kelvin.

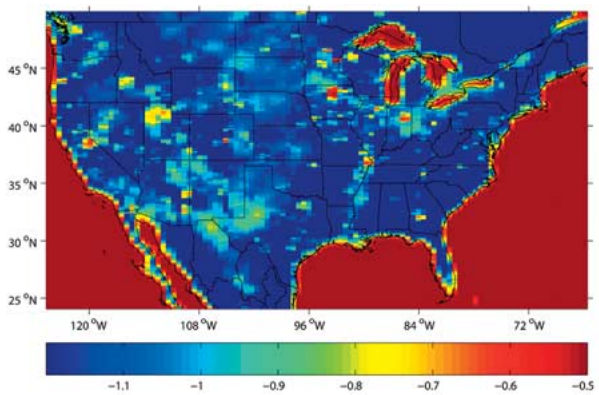

(a) C-band V excess, base10-logarithm of $(\max - P)$

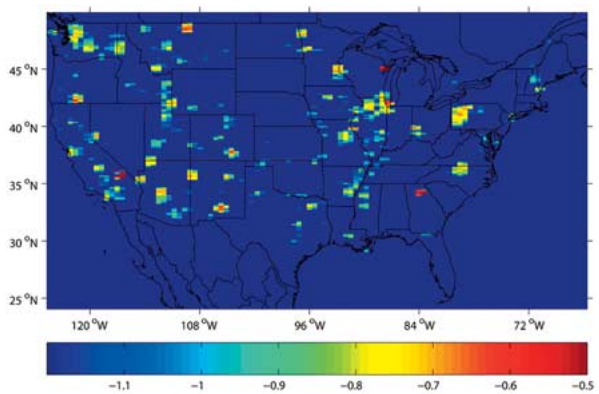

(b) C-band, H excess, base-10 logarithm $(\max P)$

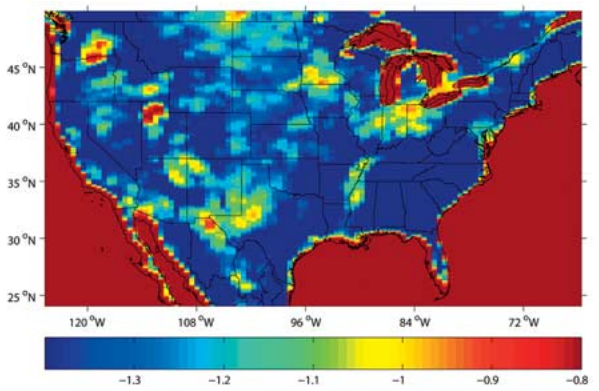

(c) X-band, V excess, base-10 logarithm of $(\max - P)$

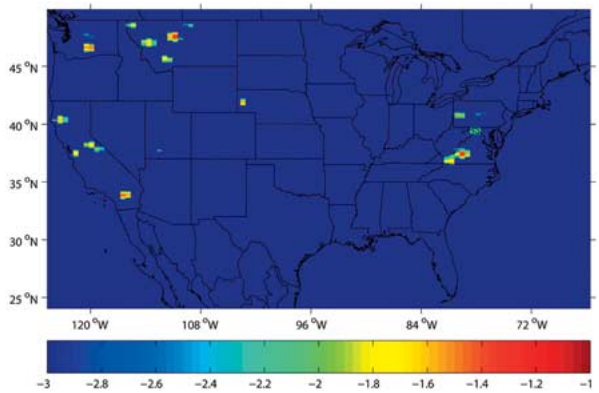

(d) X-band, H excess, base-10 logarithm of $(\max P)$

Fig. 5. Extreme values of the polarization index P.

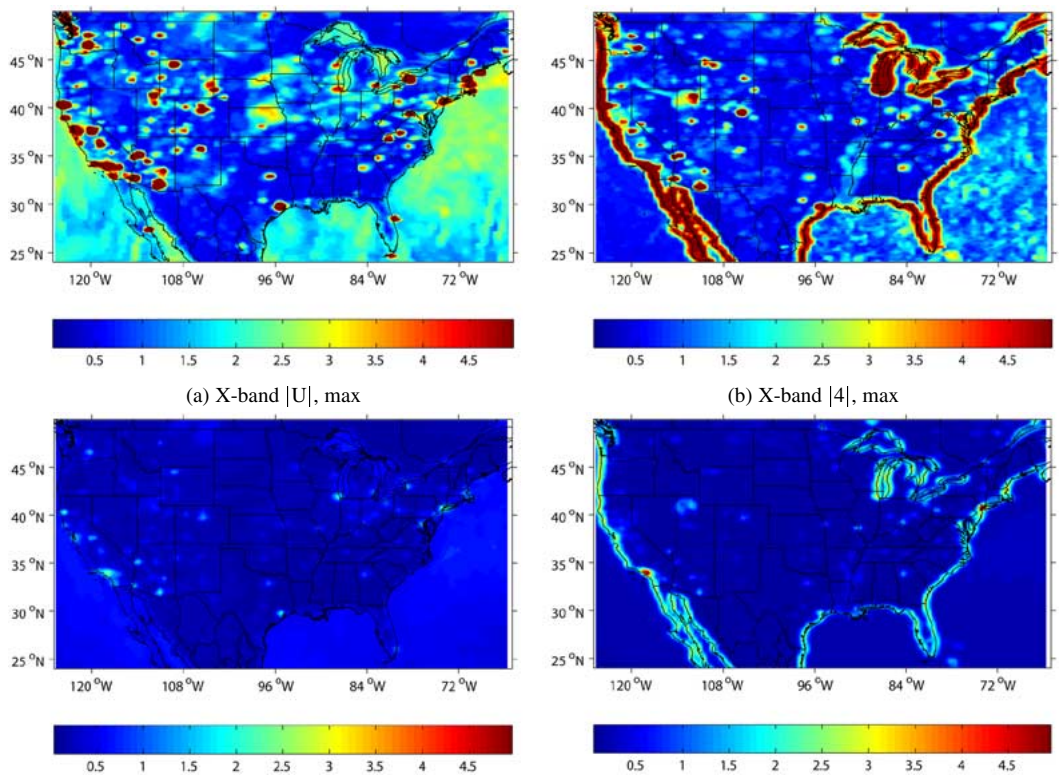

(a) X-band |U|, max

(b) X-band |4|, max

(c) X-band |U|, mean

(d) X-band |4|, mean

Fig. 6. X-band brightness temperatures (correlation channels), mean and max of amplitudes, in Kelvin.

circularly polarized antenna patterns leading to imperfect cancellation in computing the fourth Stokes parameter as the beams pass from water to land or vice versa. Evidence of this possibility was obtained from an analysis which showed that ascending and descending passes over coastal regions seem to produce fourth-Stokes brightnesses of similar magnitudes but opposite signs, as would be expected due to an antenna pattern alignment issue.

Fig. 6 reveals a much greater number of apparent RFI hot spots than observed in the X-band linear channel analyses; the number of sources observed appears more similar to those seen in the C-band results. These results indicate that the correlation channels can be used as a much-more sensitive indicator of RFI than the linear channels, because these channels should remain small under all geophysical conditions for almost all land regions when RFI is absent. This is in contrast to the X-band linear polarizations, for which geophysical variations can cause large variations in brightnesses, making RFI contributions more difficult to distinguish. These results are evidence that low-level RFI is almost certainly present the X-band linearly polarized channels, even though it was not easily detected in the linearly polarized channel studies.

Note that the locations of "hot spots" in Fig. 6 do not seem to be well correlated with the C-band hot spot locations. Furthermore, comparison of the max and mean results suggests that these emissions may be temporally intermittent in most cases, although some persistent sources are observed as well. However, another possibility that can influence the mean results is a relative azimuthal effect caused by variations in the WindSat observation angle and any preferred azimuthal angle of RFI sources.

To provide some evidence of relative azimuth effects, we investigated several of the hot spots visible in Fig. 6(c) in greater detail. Most exhibit no consistent directivity. However, a source in the vicinity of Dinsmore, CA (latitude 40.25° to 40.5° north, longitude 123.0° to 123.5° west), was seen to exhibit these effects. This is demonstrated in Fig. 7, which plots all U and fourth Stokes parameter observations falling within the above defined grid, versus the WindSat azimuthal observation angle. The data are separated into ascending (mostly northward looking) and descending (mostly southward looking) portions of the orbits. Ascending observations clearly show much stronger polarimetric brightnesses (maximum values greater than 20 K) than descending observations, and the ascending observations also show strong variations with the relative azimuthal angle. The WindSat orbit results in the majority of ascending observations being recorded in the approximate time period 9–11 A.M. local time, while the majority of the descending observations are recorded in the approximate time period 10–11:30 P.M. local time. However, the aft portion of the ascending swath also observes this source in a southerly direction in the morning overpass. Results from these data are consistent with the descending observations in Fig. 6(c), although a smaller of data points is available from the aft portion of the swath. An additional possible source of the azimuthal variations is a correlation between the Windsat azimuthal observation angle and the latitude–longitude coordinates of the observed pixel over several orbits. For example, if all WindSat observations in Fig. 7 near azimuth angle 5° were found have nearly identical spatial locations within the defined spatial grid of this source, the spatial separation between the

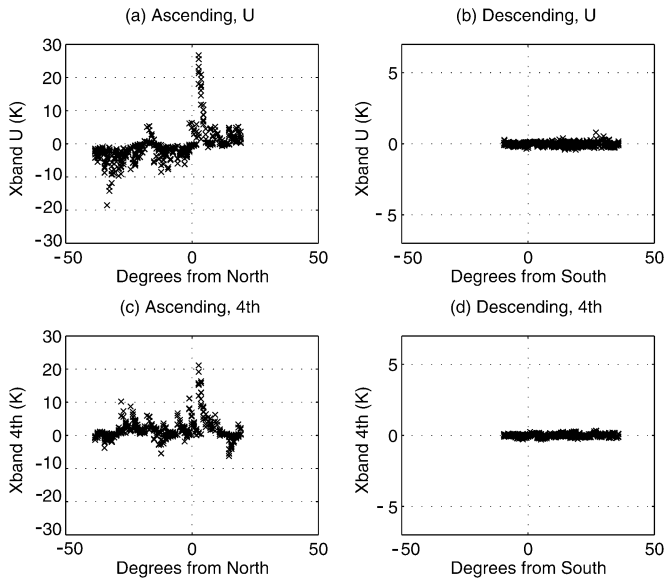

Fig. 7. X-band U observations for a directional source, versus azimuth angle.

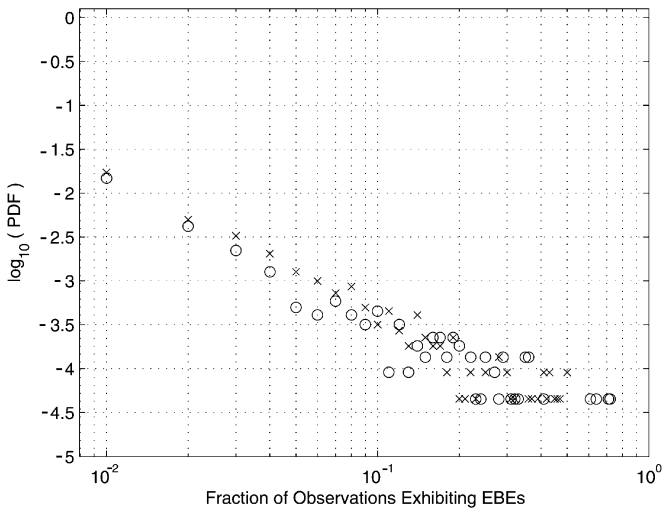

Fig. 8. PDF of the fraction of C-band observations exhibiting EBEs (observations of brightness temperature $\geq$ 330 K) per grid point. Note that the horizontal axis is plotted in log scale. (Circle) Vertical polarization. (Cross) Horizontal polarization.

WindSat observation and the interference source could be important in the results of Fig. 7. However, no such consistent dependencies were observed. Thus, it appears that directional effects of RFI sources can be observed in satellite observations. Some evidence of these effects was also provided in [1], where differences between ascending and descending overpass data were noted.

Although these results suggest that large polarimetric channel brightnesses or strong azimuthal variations of brightnesses can be useful indicators of RFI, the variations observed with azimuthal angle make it difficult for detection to be performed on a single measurement at a single azimuthal angle. In addition, typical satellite orbital geometries do not produce multiple azimuthal angle observations of a single location in one overpass, making a time history of data required in order to perform RFI analyses. This results in an RFI "masking" type procedure as has been discussed previously [1], [2]. However, the sensitivity of the RFI mask should be improved through use of the polarimetric channels. Use of the these channels for detecting low-level RFI contributions to linearly polarized brightnesses remains an interesting concept, and will be considered in more detail in future work.

IV. Temporal Analysis of Large C-Band RFI Sources

In this section we examine aspects of the temporal behavior of the interference observed, particularly for the largest C-band sources. Due to the large quantity of data and sparse temporal sampling of this six-month dataset, this is best done in a statistical manner. Due to the difficulty in detecting low-level RFI contributions, the analysis to follow focuses on the large source contributions where total measured brightnesses exceed 330 K. We refer to a single observation of a brightness temperature in excess of 330 K as an "excess brightness event" (EBE). Since EBEs were observed only in the C-band data, only the C-band data are analyzed. Furthermore, we note that this analysis is sensitive only to the strongest RFI; there are numerous cases of RFI at levels adversely affecting radiometry that are undetected in this analysis simply because the recorded brightness temperature is less than 330 K. However the analysis performed remains consistent with the goal of analyzing temporal and spatial properties of the strongest RFI sources observed.

EBE statistics for the gridded data were compiled. Fig. 8 shows the pdf of C-band EBEs over the entire six-month dataset. A few interesting conclusions can be observed from this plot. First, we note that only a tiny fraction of the grid points ever exhibit EBEs, and that no grid point shows EBEs on every observation. Only about 1% of all locations exhibit EBEs ever, and only about 0.01% of all locations exhibit EBEs most of the time. The highest rate of occurrence of EBEs was about 70%, and further analysis showed this result to occur in only one grid point in vertical polarization. Second, we note that the EBE statistics are roughly the same for both linear polarizations. Third, we observe that the pdf seems to be exhibiting a power law behavior. This is likely a function of the WindSat observational process, the gridding procedure used in generating the dataset, as well as the original RFI sources; further studies would be required in order to establish a theory predicting a power law relationship of this type.

Fig. 9 shows the rate of C-band EBEs per grid point in map form. We note here that EBE activity seems to be limited to relatively few geographical regions such as Los Angeles, CA; Seattle, WA; Tucson, AZ; Washington, PA; Winston-Salem, NC; and Connecticut, to name a few. We further note that areas of EBE activity do not appear as discrete "spikes" with respect to the grid, but rather as a distribution over a relatively large number of adjacent grid points. This is not surprising given the influence of the antenna pattern and the gridding process.

We note one more interesting feature of Fig. 9, most easily seen in the horizontal polarization results. The region bordering the Mississippi River from the Southern tip of Illinois to the northern border of Louisiana shows concentrated EBE activity in this figure. A somewhat similar feature is seen running north–south through Utah and Idaho, which very closely follows

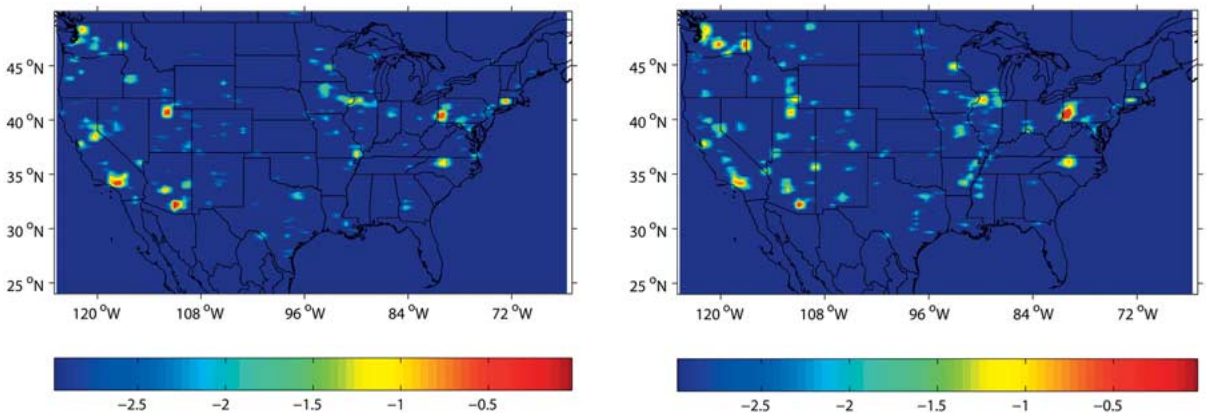

(a) Vertical polarization (b) Horizontal polarization

Fig. 9. Fraction of C-band observations exhibiting EBEs, per grid point. The color bar is labeled in $\log_{10}$ scale, i.e., "-1" corresponds to 10^{-1}, and so on.

the path of Interstate 15. Other similar linear features can be seen in central Texas and California. These results suggest that one source of EBEs may be associated with radio frequency systems in use along these transportation corridors. Similar observations were obtained with AMSR-E data in [1].

V. Conclusion and Future Work

In this paper, we presented the results of a statistical analysis of RFI observed in the continental U.S., using six months of data collected from the C- and X-band channels of WindSat. Our findings are consistent with those presented in [1] and [2], which are based on data from AMSR-E. We find that whereas much strong RFI is visible at C-band, no unambiguously detectable RFI is easily observed in the X-band V or H channels. The X-band correlation channels (U and 4) however reveal copious RFI. This is further confirmed using nominally more sensitive criteria based on spectral and polarization indexes. In all cases, a significant but imperfect correlation with population density and ground transportation corridors is noted. Comparison of max and mean data suggests that many of the RFI sources are persistent. Harder to establish is the actual variability of the RFI, because of the sparse temporal sampling of the Earth's surface. We observed at least one instance in which an X-band RFI source was seen to exhibit strong directivity in azimuth. In terms of geographic distribution, we confirm the findings of [1] that RFI is observed primarily within the U.S., with much less evidence seen in Canada, Mexico, or at sea.

Although previous methods for developing RFI masks appear applicable to this dataset as well, no obvious means for detecting low-level RFI in single observations is available at present. The strong sensitivity of the correlation channels to land-based RFI suggests that further work should examine use of the correlation channels, as well as the spectral indexes, for development of such algorithms. Matchup studies against existing databases of RFI sources will be used in future studies to examine possible techniques. However, improved knowledge of RFI source temporal and directional properties beyond those available in existing databases would also assist in this process. Because the data analyzed are brightness temperatures integrated over very large bandwidths for a few milliseconds, it is not possible to observe the waveform(s) of the observed RFI. Coherently sampled waveform data would be very helpful in identifying the source(s) of the RFI and further resolving spectral and temporal characteristics, which are potentially useful for developing mitigation techniques. For this reason, we have embarked on a project to collect coherent waveform data in parallel with airborne radiometric measurements at C-band [7]. Data have already been collected over portions of the U.S. and are currently being analyzed.

Acknowledgment

The authors thank the Naval Research Laboratory (NRL) WindSat team (led by P. Gaiser) for providing the WindSat data used in this study. L. Li (NRL) is also thanked for providing a preprint of [2].

References

[1] L. L. Li *et al.*, "A preliminary survey of radio-frequency interference over the U.S. in Aqua AMSR-E data," *IEEE Trans. Geosci. Remote Sens.*, vol. 42, no. 2, pp. 380–380, Feb. 2004.

[2] E. G. Njoku, P. Ashcroft, T. K. Chan, and L. Li, "Global survey and statistics of radio-frequency interference in AMSR-E land observations," *IEEE Trans. Geosci. Remote Sens.*, vol. 43, no. 5, pp. 938–938, May 2005.

[3] D. B. Kunkee, N. S. Chauhan, and J. J. Jewell, "Spectrum management for the NPOESS Conical-scanning Microwave Imager/Sounder (CMIS)," in *Proc. IGARSS*, vol. 2, 2002, pp. 1002–100.

[4] P. W. Gaiser *et al.*, "The Windsat spaceborne polarimetric microwave radiometer: Sensor description and early orbit performance," *IEEE Trans. Geosci. Remote Sens.*, vol. 42, no. 11, pp. 2347–2361, Nov. 2004.

[5] J. F. Galantowicz, A. Lipton, and S. A. Boukabara, "Options for C band RFI mitigation: Analysis of potential improvements in radiance estimation and soil moisture retrieval," presented at the *IEEE Geoscience and Remote Sensing Symp.*, Anchorage, AK, 2004.

[6] L. Li, P. W. Gaiser, and M. Bettenhausen, "WindSat radio-frequency interference signature and its identification over land and ocean," *IEEE Trans. Geosci. Remote Sens.*, vol. 44, no. 3, pp. 530–539, 2006.

[7] J. T. Johnson, A. J. Gasiewski, B. Guner, G. A. Hampson, S. W. Ellingson, R. Krishnamachari, N. Niamsuwan, E. McIntrye, M. Klein, and V. Leuski, "Airborne radio frequency interference studies at C-band using a digital receiver," *IEEE Trans. Geosci. Remote Sens.*, 2006, to be published.

Steven W. Ellingson (S'87–M'90–SM'03) received the B.S. degree in electrical and computer engineering from Clarkson University, Potsdam, NY, in 1987, and the M.S. and Ph.D. degrees in electrical engineering from The Ohio State University (OSU), Columbus, in 1989 and 2000, respectively.

From 1989 to 1993, he served on active duty with the U.S. Army, attaining the rank of Captain. From 1993 to 1995, he was a Senior Consultant with Booz-Allen and Hamilton, McLean, VA. From 1995 to 1997, he was a Senior Systems Engineer with Raytheon E-Systems, Falls Church, VA. From 1997 to 2003, he was a Research Scientist with the ElectroScience Laboratory, OSU. Since 2003, he has been an Assistant Professor in the Bradley Department of Electrical and Computer Engineering, Virginia Polytechnic Institute and State University, Blacksburg, VA. His research interests include antennas and propagation, applied signal processing, and instrumentation.

Joel T. Johnson (S'91–M'96–SM'03) received the B.E.E. degree from the Georgia Institute of Technology, Atlanta, in 1991, and the S.M. and Ph.D. degrees from the Massachusetts Institute of Technology, Cambridge, in 1993 and 1996, respectively.

He is currently a Professor in the Department of Electrical Engineering and ElectroScience Laboratory, The Ohio State University, Columbus. His research interests are in the areas of microwave remote sensing, propagation, and electromagnetic wave theory.

Dr. Johnson is a member of International Union of Radio Science (URSI) Commissions B and F, as well as a member of Tau Beta Pi, Eta Kappa Nu, and Phi Kappa Phi. He received the 1993 Best Paper Award from the IEEE Geoscience and Remote Sensing Society, was named an Office of Naval Research Young Investigator, National Science Foundation Career awardee, and PECASE Award recipient in 1997, and was recognized by the U.S. National Committee of URSI as a Booker Fellow in 2002.